Structural and Biochemical Characterization of *Xylella fastidiosa* DsbA Family Members: New Insights into the Enzyme−Substrate Interaction[†,‡]

Fábio C. Rinaldi, Andréia N. Meza, and Beatriz G. Guimarães*

Brazilian Synchrotron Light Laboratory—LNLS, Campinas, Brazil

Received October 9, 2008; Revised Manuscript Received February 25, 2009

ABSTRACT: Disulfide oxidoreductase DsbA catalyzes disulfide bond formation in proteins secreted to the periplasm and has been related to the folding process of virulence factors in many organisms. It is among the most oxidizing of the thioredoxin-like proteins, and DsbA redox power is understood in terms of the electrostatic interactions involving the active site motif CPHC. The plant pathogen *Xylella fastidiosa* has two chromosomal genes encoding two oxidoreductases belonging to the DsbA family, and in one of them, the canonical motif CPHC is replaced by CPAC. Biochemical assays showed that both *X. fastidiosa* homologues have similar redox properties and the determination of the crystal structure of *Xf*DsbA revealed substitutions in the active site of *X. fastidiosa* enzymes, which are proposed to compensate for the lack of the conserved histidine in *Xf*DsbA2. In addition, electron density maps showed a ligand bound to the *Xf*DsbA active site, allowing the characterization of the enzyme interaction with an 8-mer peptide. Finally, surface analysis of *Xf*DsbA and *Xf*DsbA2 suggests that *X. fastidiosa* enzymes may have different substrate specificities.

An essential step in the folding process of many proteins is the formation of disulfide bonds. In prokaryotes, the Dsb[1] system is responsible for the oxidation of cysteine residues in a catalyzed process divided into two pathways: the DsbA-based oxidation pathway and the DsbC-based isomerization pathway (reviewed in ref (*1*)). Initially identified in *Escherichia coli* (*2*), DsbA is a catalyst of disulfide bond formation in the periplasm. As a member of the thioredoxin superfamily, the DsbA crystal structure revealed a two-domain protein, showing a helical domain inserted into a thioredoxin-like fold (*3*). Its extremely oxidizing nature (*4, 5*) relies on the stabilization of the catalytic cysteine thiolate which is a result of hydrogen bond and electrostatic interactions involving the active site motif CPHC (*6*). In particular, the active site histidine has been shown to be essential for maintenance of DsbA redox potential (*7*). Until the recent characterization of the DsbL protein from uropathogenic *E. coli* strain CFT073 (*8*), DsbA was known as the most oxidizing of the thioredoxin-like proteins. DsbL shares structural and functional similarities with DsbA, but it is proposed to have a more limited set of specific substrates (*8*).

Using an approach that intends to simulate natural selection, Quan and co-workers recently showed that the CXXC motif is a major factor in determining the function of the thioredoxin-like proteins (*9*). Identification of thioredoxin mutants with the ability to complement DsbA deletion in *E. coli* revealed that, in such mutants, a positively charged residue frequently appears within the CXXC motif and a proline residue is favored as the N-terminal amino acid of the XX sequence (*9*). In addition, results obtained by Quan and colleagues revealed that the CXXC sequence has the ability not only to control the redox potential of thioredoxin-related proteins but may also confer disulfide isomerase activity and has important effects on the protein ability to interact with its redox partners (*9*).

Although a large amount of genetic, biochemical, and structural information on DsbA proteins is available, new findings keep challenging the complete understanding of the functional role of DsbA family members and their molecular mechanism. Analysis of the genome of the Gram-negative bacterium *Xylella fastidiosa* (*10*), a plant pathogen that causes economically important diseases in citrus, grapevine, and coffee, revealed the presence of two adjacent chromosomal genes coding for two DsbA-like proteins. We were intrigued by the presence of these two *dsbA* genes (codes XF1436 and XF1437) in *X. fastidiosa* genome, since DsbA homologue XF1437 possesses a CPAC cluster at the active site, in place of the canonical DsbA motif CPHC. Recently, a second disulfide oxidoreductase homologue to DsbA was identified in the cold-adapted bacterium *Pseudoalteromonas haloplanktis* TAC 125 (*Ph*TAC125) (*11*). Interestingly, *Ph*TAC125 possesses two adjacent chromosomal *dsbA* genes organized in a functional operon. In a classical complemen-

[†] This work was supported by FAPESP Grants CEPID/CBME 98/14138-2 and SMolBNet 00/10266-8. F.C.R. is recipient of a FAPESP Ph.D. fellowship (03/12875-0). Use of the National Synchrotron Light Source was supported by the National Institutes of Health National Center for Research Resources to the Brookhaven Biology Department and National Synchrotron Light Source and in part by support from the Department of Energy Office of Biological and Environmental Research Energy, Basic Energy Sciences.

[‡] The coordinates for the DsbA from *Xylella fastidiosa* (*Xf*DsbA) have been deposited in the Brookhaven Protein Data Bank with the accession number 2REM.

* Address corresponding to this author at Synchrotron SOLEIL, L'Orme des Merisiers, Saint-Aubin, BP 48, 91192 Gif-sur-Yvette Cedex, France. Tel: +33 (0)1 69 35 97 94. Fax: +33 (0)1 69 35 94 56. E-mail: beatriz.guimaraes@synchrotron-soleil.fr.

[1] Abbreviations: Dsb, disulfide bond; GSH, reduced glutathione; GSSG, oxidized glutathione; DTT, dithiothreitol; EDTA, ethylenediaminetetraacetic acid.

10.1021/bi801899x CCC: $40.75
Published on Web 02/26/2009

tation assay, both *Ph*DsbA and *Ph*DsbA2 proteins were able to restore the cellular motility of *E. coli dsbA* null mutants (*11*), indicating that both proteins may possess disulfide oxidoreductase activity. Similarly to what we had encountered for the *X. fastidiosa* homologues, *Ph*DsbA contains the conserved motif CPHC while, in *Ph*DsbA2 active site, the histidine residue is substituted by an alanine (CPAC).

Heras and co-workers recently determined the first crystal structure of a DsbA family member from a Gram-positive bacterium (*12*). *Staphylococcus aureus* DsbA (*Sa*DsbA) also lacks residues predicted to be important for DsbA function, presenting motifs that are more typical of the Gram-negative disulfide isomerases. Structural and functional analysis of *Sa*DsbA revealed that *S. aureus* uses a different mechanism to that of *E. coli* for oxidizing disulfides in secreted proteins (*12*).

Aiming to investigate the functional properties of the two *X. fastidiosa* DsbA proteins and to verify the putative differences due to the histidine substitution within the active site, we produced both *Xf*DsbA and *Xf*DsbA2 recombinant proteins and performed structural and biochemical studies. The results presented in this work show that, despite the absence of the active site histidine in *Xf*DsbA2, both proteins have similar redox potentials. In addition, the crystal structure of *Xf*DsbA solved at 1.9 Å resolution revealed significant differences in the interactions involving the catalytic Cys37 between *Xf*DsbA and its homologues.

EXPERIMENTAL PROCEDURES

Construction of Expression Vectors. The coding sequences of XF1436 and XF1437, named *Xf*DsbA and *Xf*DsbA2 (NCBI accession numbers 1126982 and 1126983, respectively), excluding the signal peptides, were initially PCR-amplified from the *Xylella fastidiosa* genomic DNA using oligonucleotides XF1436R (5′-CTCGAGTCACCGGCCATGTGAGGCAG-3′), XF1436F (5′-CATATGAATCACCTTCCGGTTGTTGG-3′), XF1437R (5′-CTCGAGCTACTTACCAAGCGACTTACGC-3′), and XF1437F (5′-CATATGCAAGCTAAGGATGGTAGTGCGG-3′), containing the *Nde*I and *Xho*I restriction sites. The cDNA was inserted into the pGEM-T-easy vector (Promega), and the sequences were verified by DNA sequencing analysis using an ABI Prism 377 DNA sequence analyzer (Applied Biosystems). Subsequently, the cDNA were transferred to the *E. coli* expression vector pET28a(+) (Novagen, Inc.), using the *Nde*I and *Xho*I restriction sites. Site-directed mutageneses were produced using the QuikChange site-directed mutagenesis kit (Stratagene). The *Xf*DsbA and *Xf*DsbA2 variants were constructed by PCR amplification of the wild-type coding sequence using plasmid pET28a(+)-*Xf*DsbA (or *Xf*DsbA2) as DNA template and primers containing the base substitutions to produce the mutants *Xf*DsbA^{T157V} and *Xf*DsbA2^{T203V}. The resulting PCR products were submitted to sequence analysis to verify the bases' substitutions.

Expression and Purification. XfDsbA and *Xf*DsbA2 were expressed in *E. coli* strain C43 (DE3) (Avidis). Cells were grown at 37 °C in 1 L of LB medium containing kanamycin (50 mg/L). Recombinant proteins were produced in the *E. coli* cytoplasm, and protein expression was induced by the addition of 0.4 mM IPTG (isopropyl β-D-thiogalactopyranoside) when the cell culture reached an optical density of 0.8 at 600 nm. After 6 h, cells were harvested by centrifugation (30 min, 3000*g*, 4 °C), and the pellet was suspended in 20 mL of buffer A (20 mM sodium phosphate, pH 7.4, 500 mM sodium chloride, 5 mM imidazole). Cells were disrupted by sonication, and unbroken cells and debris were removed by centrifugation (30 min, 20000*g*). DNA was precipitated with 2% (w/v) streptomycin sulfate during 45 min and removed by centrifugation (30 min, 3000*g*, 4 °C). Recombinant *Xf*DsbA and *Xf*DsbA2 were purified in two chromatography steps. Total extracts were injected on a 5 mL HiTrap chelating column (GE Healthcare) using an ÄKTA-FPLC system set at a flow rate of 1.5 mL/min. The column was washed with 6 CV (column volume) of buffer A and eluted with a linear gradient of 0−100% buffer B (buffer A containing 1 M imidazole) in 12 CV. *Xf*DsbA and *Xf*DsbA2 were further purified by gel filtration chromatography. For this purpose, affinity-purified proteins were concentrated, loaded onto a HiLoad 16/60 Superdex 75 gel-filtration column (Amersham Pharmacia), and eluted with buffer C (100 mM sodium phosphate, pH 6.8, 200 mM sodium chloride) at a flow rate of 1.0 mL/min. Purified proteins were dialyzed against 10 mM Tris-HCl, pH 7.5, and 20 mM NaCl, and protein concentration was estimated from direct absorbance at 280 nm considering an extinction molar coefficient of 21740 and 26025 M^{-1} cm^{-1} at 280 nm for *Xf*DsbA and *Xf*DsbA2, respectively. Expression and purification of mutants *Xf*DsbA^{T157V} and *Xf*DsbA2^{T203V} followed the same procedures used for wild-type enzymes. The selenomethionine-labeled *Xf*DsbA (SeMet-*Xf*DsbA) was produced in the same *E. coli* strain used for nonlabeled protein expression. Cells were grown in M9 minimal medium (6.8 g/L Na_2HPO_4, pH 7.3, 3 g/L KH_2PO_4, 0.5 g/L NaCl, 2 mM $MgSO_4$, 1% (w/v) glucose, 100 μM $CaCl_2$, 30 μM thiamin, 18.7 mM NH_4Cl) containing 50 μM $FeCl_3$, 10 μM $MnCl_2$, 10 μM $ZnCl_2$, 2 μM $CoCl_2$, and 50 mg/L kanamycin, under agitation until the optical density of the culture reached 0.8 at 600 nm. The culture was then supplemented with lysine, phenylalanine, and threonine (100 mg/L), isoleucine and valine (50 mg/L), and selenomethionine (50 mg/L) 15 min before induction with 0.4 mM IPTG for 6 h at 37 °C. SeMet-*Xf*DsbA was purified using the same protocol as described above, and selenomethionine incorporation was confirmed by mass spectrometry, which indicated that the three methionines of *Xf*DsbA were replaced by selenomethionines (data not shown).

*Crystallization and Data Collection. Xf*DsbA was concentrated to 11 mg/mL and incubated with 5 mM DTT for 60 min to maintain the protein in a homogeneous state suitable for crystallization procedures. *Xf*DsbA was crystallized by the sitting-drop vapor-diffusion method at 20 °C. Initial crystallization trials were performed using Crystal Screen, Crystal Screen II (Hampton Research), Wizard I and II (Emerald Biosystems), and JBScreen Classic 1-8 (Jena Bioscience). Equal volumes (2.0 μL) of protein sample and reservoir solution were mixed for crystallization and equilibrated against 600 μL of reservoir solution. Needle-shaped crystals grew in 0.1 M sodium citrate, pH 5.6, 0.1 M ammonium sulfate, and 30% PEG 4000. Crystallization was further optimized by varying the buffer pH and testing PEG 4000 concentration ranging from 10% to 35% and ammonium sulfate from 0 to 250 mM. Optimal condition was obtained with the reservoir solution consisting of 0.1 M

Table 1: Data Collection and Refinement Statistics

	native	SeMet
Data Collection Statistics		
space group	*C*2	*C*2
unit cell		
a, *b*, *c* (Å)	200.12,41.72,79.81	203.16,42.54,81.43
β (deg)	95.87	96.15
wavelengh (Å)	1.431	0.9795
resolution range (Å)	50.00−1.90(1.97−1.90)	50.00−1.85(1.92−1.85)
no. of reflections/no. of unique reflections	52137/14898	
redundancy	3.5(2.9)	6.6(4.9)
completeness (%)	99.7(98.3)	91.5(83.6)
R_{symm} (%)	7.4(47.9)	7.9(31.3)
$I/\sigma(I)$	14.7(2.0)	22.6(8.9)
no. of seleniums (assym unit)		6
Refinement Statistics		
resolution range (Å)	50.0−1.90	
no. of reflections (working data/test data)	14136/761	
R-factor (%)[a]	18.3(24.5)	
R-free (%)[b]	22.4(32.7)	
figure of merit[c]	0.87	
protein atoms	4452	
water molecules	516	
mean *B* value/Wilson *B* (protein, all atoms) (A^2)	24.9/21.8	
mean *B* value (8-mer peptide, all atoms)	39.8	
mean *B* value (solvent) (A^2)	26.9	
rmsd bond length (Å)	0.011	
rmsd bond angle (deg)	1.288	

[a] *R*-factor $= \sum_{hkl}||F_o| - k|F_c||/\sum_{hkl}|F_o|$. [b] *R*-free was computed identically, except that 5% of the reflections were omitted as a test set. [c] Figure of merit (*m*) is $m = |F(hkl)_{best}|/|F(hkl)|$, where $F(hkl)_{best} = \sum_\alpha P(\alpha)F_{hkl}(\alpha)/\sum_\alpha P(\alpha)$; $P(\alpha)$ is the probability distribution for the phase angle α.

sodium citrate, pH 5.0, and 30% PEG 4000. Drops were made of 4.5 μL of protein sample mixed with an equal volume of reservoir solution and 1 μL of 1 M guanidine hydrochloride used as additive. The crystals reached approximately 150 × 150 × 75 μm^3 after 10−15 days. SeMet-*Xf*DsbA was crystallized in the same condition used for nonlabeled protein.

Nonlabeled *Xf*DsbA crystals were soaked during 3 s in a cryoprotectant solution containing the mother liquor (0.1 M sodium citrate, pH 5.0, and 30% PEG 4000) supplemented with 20% glycerol prior to flash-cooling in a 100 K nitrogen gas stream. Native X-ray diffraction data were collected at the protein crystallography beam line D03B-MX1 of the Brazilian Synchrotron Light Laboratory, LNLS, Campinas, Brazil. The wavelength was set to 1.43 Å, and a MARCCD detector was used to record the rotation data. Data from SeMet-*Xf*DsbA crystals were collected at the X26C beam line of the National Synchrotron Light Source, BNL, Brookhaven, USA, using an ADSC Quantum-4 detector. Diffraction data were collected at a single wavelength (0.9795 Å) corresponding to the maximum of *f*″. Native and derivative data sets were processed using the program HKL2000 (*13*). Crystals belong to space group *C*2, and Matthews coefficient calculation (*14*) indicated the presence of three monomers in the asymmetric unit, giving a V_M value of 2.39 $Å^3$ Da^{-1} and a solvent content of 45%. Table 1 summarizes data collection statistics.

Structure Solution and Refinement. Extensive attempts to solve the *Xf*DsbA structure by molecular replacement methods using the available structures of *E. coli* DsbA (PDB codes 1A2L, 1DSB, 1FVK, and 1A2J) and *Vibrio cholerae* DsbA (PDB code 1BED) as search models were unsuccessful. *Xf*DsbA structure was then solved by single-wavelength anomalous dispersion (SAD) using the SeMet derivative data set. Six Se sites were found with the program SHELXD (*15*), and refinement of heavy atom parameters and calculation of phases were carried out with SHARP (*16*). After density modification with the program SOLOMON (*17*) the good quality of the electron density map allowed the automatic building by the program ARP/wARP (*18*) of 12 polypeptide chain fragments containing a total of 536 residues (out of 582 expected for three monomers).

The native data set was used for structure refinement, which was carried out with REFMAC (*19*). The model was manually built to completion using the program Coot (*20*), and refinement cycles were alternated with visual inspection of the electron density maps and model rebuilding. During the final cycles water molecules were added using the program ARP/wARP, and the ligand was modeled. Translation/libration/screw (TLS) refinement were performed using TLS groups defined by the TLSMD server (*21*). One TLS group per monomer was used in refinement, which converged to R_{factor} and R_{free} values of 0.18 and 0.22, respectively, with good overall stereochemistry. As defined by the program PROCHECK (*22*) all non-glycine and non-proline residues fall in the most favored or additionally allowed regions of the Ramachandran plot. Table 1 summarizes the refinement statistics. Figures were produced using the program Pymol (*23*).

Determination of Redox Potential. The redox potentials of wild-type *Xf*DsbA and *Xf*DsbA2 and mutants were determined following the procedure described by Wunderlich and Glockshuber (*4*). This method is based on the increase of the intrinsic tryptophan fluorescence of DsbA upon reduction of the enzyme. Fluorescence experiments were performed on an ISS K2 fluorometer (Champaign, IL). The redox equilibrium of the proteins with the glutathione system was studied in the range from pH 6.0 to pH 8.0, in the following buffers: pH 6.0 and 7.0, 100 mM sodium phosphate; pH 8.0, 100 mM Tris-HCl. Buffers contained 1 mM

EDTA, and all solutions used were degassed and flushed with nitrogen to avoid air oxidation. The fluorescence intensities were measured at 333 nm (excitation wavelength 280 nm) where the difference between the emission of oxidized and reduced proteins is maximal (increase of 50% and 60% upon reduction of *Xf*DsbA and *Xf*DsbA2, respectively; data not shown). After purification, the fluorescence intensity of the pure enzyme was compared with the emission of a sample treated with 25 mM diamide, to guarantee that the protein was fully oxidized. Oxidized DsbA (0.5 μM) was incubated at 30 °C in the presence of 0.1 mM GSSG and different concentrations of GSH (0−2.4 mM). Incubation times necessary for the reactions to reach the equilibrium were determined for each pH (6.0, 14 h; 7.0, 7 h; 8.0, 1 h). Three independent measurements were performed at each pH, and the data were fitted according to eq 1.

$$R = \frac{[\mathrm{GSH}]^2/[\mathrm{GSSG}]}{K_{eq} + [\mathrm{GSH}]^2/[\mathrm{GSSG}]} \quad (1)$$

The values of R were determined according to the equation $R = (F - F_{ox})/(F_{red} - F_{ox})$, where F is the measured fluorescence intensity and F_{ox} and F_{red} are the fluorescence intensities of completely oxidized and reduced DsbA, respectively. The equilibrium constant K_{eq} was obtained from the transition curve fit (eq 1). Based on the redox potential of the pair GSH/GSSG calculated according to eq 2 (*4*), *Xf*DsbA and *Xf*DsbA2 redox potentials were determined by the Nernst equation (eq 3).

$$E_0^{pH} = E_0' - 60.2\ \mathrm{mV}\ (\mathrm{pH} - 7) \quad (2)$$

$$E_{0\,\mathrm{DsbA}} = E_{0\,\mathrm{GSH/GSSG}} - (RT/nF) \ln K_{eq} \quad (3)$$

where R is the gas constant (8.315 J K^{-1} mol^{-1}), T is the absolute temperature (303.15 K), n is the number of transferred electrons ($n = 2$), and F is the Faraday constant (9.649×10^4 C mol^{-1}). $E_{0\,\mathrm{GSH/GSSG}}$ was determined at 25 °C and pH 7.0 (−0.240 V) by Rost and Rapoport (*24*). The redox potential of the glutathione couple at different pH was calculated using the redox potential at pH 7.0 and applying eq 2 (pH 6.0, −0.180 V; pH 7.0, −0.240 V; pH 8.0, −0.300 V).

Molecular Modeling of XfDsbA2. *Xf*DsbA2 homology model was built using the program Modeler (*25*). Atomic coordinates of *Xf*DsbA were used as template. *Xf*DsbA2 amino acids corresponding to the signal peptide and an additional 44 N-terminal residues which are not present in *Xf*DsbA sequence were excluded. Alignment performed by the program Modeler, based on the structure of the template, resulted in sequence identity of 41%. Five models were generated and optimized by simulated annealing procedures. The model presenting the lowest "objective function" (*25*) was selected as the best model and submitted to validation using external evaluation programs. Model validation was performed using the programs PROCHECK (*22*), VERIFY3D (*26*), and PROVE (*27*).

RESULTS

Overall Structure of X. fastidiosa DsbA. Wild-type and selenomethionine-labeled *Xf*DsbA were produced, purified, and crystallized. The crystal structure of *Xf*DsbA was solved by single-wavelength anomalous diffraction and refined at 1.9 Å resolution to a final R_{factor} of 0.183 (R_{free} = 0.224). The *Xf*DsbA final atomic model includes three monomers (referred to as A, B, and C) in the asymmetric unit, and the quality of the electron density maps allowed modeling of residues 4 to 193 in monomer A (out of 194), 4 to 190 in monomer B, and 3 to 193 in monomer C. Superposition of the symmetrically independent monomers results in overall rms deviations of 0.30−0.38 Å (all Cα aligned). Structural analysis and comparisons with homologous structures were performed using monomer A, unless stated otherwise. As expected, *Xf*DsbA shows a two-domain structure as described for the DsbA family (*3*). A four-helix domain (α2 to α5) is inserted into a thioredoxin-like fold, which is composed by a central β-sheet (antiparallel strands β1−β5) flanked by helices α1, α6, and α7. Helix α6 and the loop linking α2 and β3 connect the two domains (Figure 1).

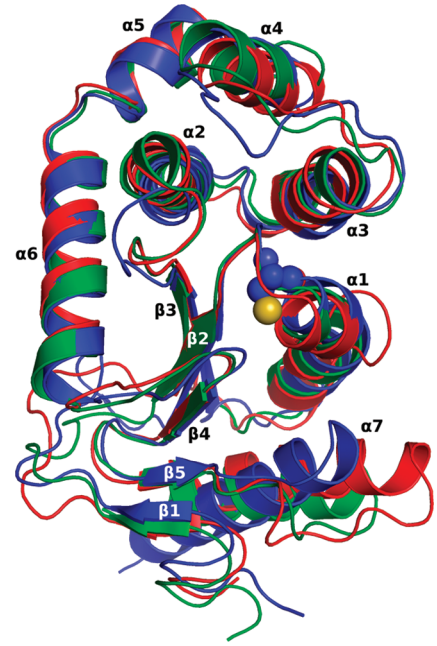

FIGURE 1: Overall structural comparison. *Xf*DsbA is represented in blue, *Ec*DsbA (PDB code 1A2L, reduced state) is shown in red, and *Vc*DsbA (PDB code 1BED, oxidized state) is shown in green. The catalytic Cys38 of *Xf*DsbA is represented with spheres.

Superposition of structures of *Xf*DsbA and its counterparts from *E. coli* (*Ec*DsbA, 21% sequence identity, PDB code 1A2L) (*6*) and *V. cholerae* (*Vc*DsbA, 23% sequence identity, PDB code 1BED) (*28*) resulted in overall rms deviations of 2.1 Å (169 Cα aligned) and 1.9 Å (169 Cα aligned), respectively. Comparison of the thioredoxin and helical domains of *Xf*DsbA with the equivalent domains of *Ec*DsbA and *Vc*DsbA resulted in overall rms deviations of 2.1 Å (97 Cα aligned)/1.3 Å (73 Cα aligned) (thioredoxin domain/helical domain) and 1.9 Å (98 Cα aligned)/1.7 Å (74 Cα aligned) (thioredoxin domain/helical domain), respectively.

Major structural differences reside in the loops. The *Xf*DsbA loop connecting strands β1 and β2 is five residues longer than in *Ec*DsbA and *Vc*DsbA, and the loop connecting helices α3 and α4 shows an insertion of three residues (see alignment in Supporting Information Figure S1), making this loop more prominent in *Xf*DsbA than in *Ec*DsbA and *Vc*DsbA (Figure 1). A structural change is observed in the

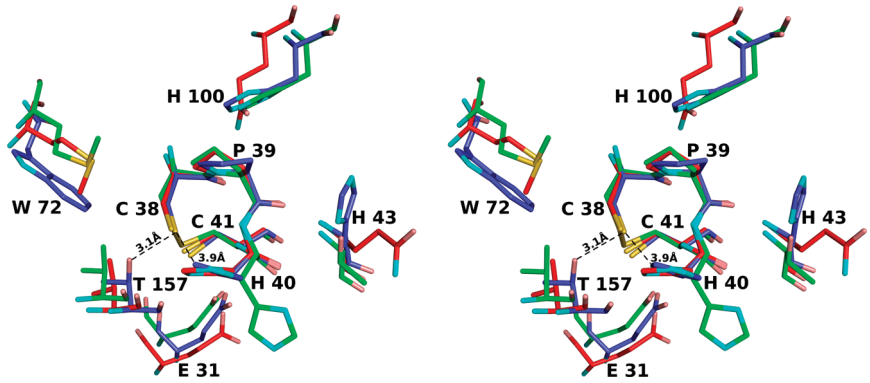

FIGURE 2: Stereoview of the superposition of the active sites of *Xf*DsbA, *Ec*DsbA, and *Vc*DsbA. The C atoms of *Xf*DsbA, *Ec*DsbA, and *Vc*DsbA are represented in blue, red, and green, respectively. Labels and distances refer to *Xf*DsbA residues. Interactions of the N-terminal cysteine (Cys38) with Thr157 and His40 are highlighted.

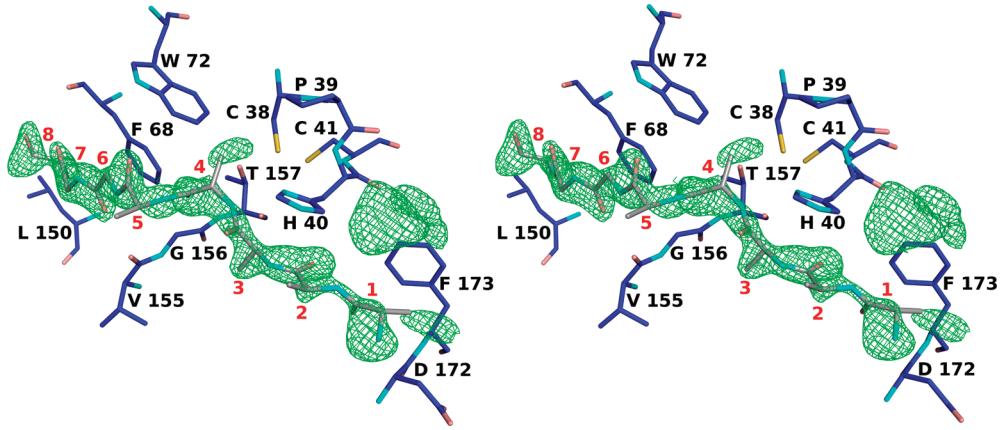

FIGURE 3: Stereoview of the *Xf*DsbA monomer C active site showing the modeled 8-mer peptide. The $F_o - F_c$ map contoured at 3σ (green) is superposed to the final model. The CPHC motif and the residues involved in interactions with the polypeptide are labeled, and the peptide units are numbered in red.

loop between β3 and α2, which connects the two DsbA domains (Figure 1). The *Xf*DsbA β3-α2 loop is two residues shorter than in *Ec*DsbA and *Vc*DsbA, and its conformation moves the *Xf*DsbA main chain away from the catalytic cysteine. The side chain of Trp72, which is located at the end of the loop, approaches the active site and structurally replaces a methionine residue found in *Ec*DsbA and *Vc*DsbA (Figure 2). Interestingly, this loop participates in the formation of the well-characterized DsbA hydrophobic patch and was shown to be involved in DsbA−DsbB interaction in *E. coli* (*29, 30*). In addition, the loop connecting strand β5 and helix α7 is highly variable among the three structures. Compared with *Ec*DsbA, the β5-α7 loop of *Xf*DsbA presents a deletion of six residues as well as in *Vc*DsbA, where helix α7 is shortened by one turn (see alignment in Supporting Information Figure S1). *Xf*DsbA α7 is four residues longer than in *Ec*DsbA and points in the direction of the active site, placing the Phe173 residue close to the active site His40, in position to participate in the hydrophobic groove (discussion below). Finally, similarly to *Vc*DsbA, *Xf*DsbA does not present a kink in helix α1. The kink which splits *Ec*DsbA α1 in two helices is caused by the insertion of three residues (Glu38, Val39, Leu40), which are structurally replaced by Pro39 in *Vc*DsbA and Ser46 in *Xf*DsbA (see alignment in Supporting Information Figure S1).

Structural superposition of *Xf*DsbA and DsbL from uropathogenic *E. coli* strain CFT073 (18% sequence identity, PDB code 3C7M) (*8*) resulted in an overall rms deviation of 2.4 Å (169 Cα aligned). Superposition of the two domains separately resulted in overall rms deviations of 2.3 Å for the thioredoxin domain (100 Cα aligned) and 2.3 Å for the helical domain (73 Cα aligned). Main differences are encountered in the loops. The loop connecting β3 and α2 is slightly more open in *Xf*DsbA than in DsbL, and *Xf*DsbA Trp72 is replaced by the structurally equivalent Lys61 in DsbL, conferring a positive charge to DsbL in this region. The loop between helices α3 and α4 is highly variable among DsbA homologues (see Figure 1 and alignment in Supporting Information Figure S1). In DsbL, the equivalent loop is interrupted by a 3_{10}-helix characterized by the presence of acidic residues, whereas the corresponding sequence in *Xf*DsbA shows the presence of noncharged residues. Finally, the long loop connecting DsbL helices α2 and α3 is not present in *Xf*DsbA, and *Xf*DsbA helix α7, also variable among DsbA homologues, is longer than the equivalent helix of DsbL.

Active Site of XfDsbA. The crystal structure of *Xf*DsbA was determined at pH 5.0 from a protein treated with DTT prior to crystallization. The three symmetrically independent monomers of *Xf*DsbA present the catalytic cysteines in the reduced state, and the conformation of the active site residues is very similar in the three monomers (Supporting Information Figure S2). Despite the overall similarity, structural comparison of *Xf*DsbA with its counterparts from *E. coli* and *V. cholerae* reveals some interesting differences in their active sites. Comparisons were performed with reduced *Ec*DsbA (PDB code 1A2L) and oxidized *Vc*DsbA (PDB code

1BED), since there is no crystallographic structure of *Vc*DsbA available in the reduced state.

The *Xf*DsbA Cys38 thiolate (equivalent to Cys30 in *Ec*DsbA) is stabilized by hydrogen bonds with the backbone amide nitrogens of Gly35 (3.0 Å distance), Cys41 (3.2 Å), and Ala42 (3.0 Å) and with the thiol of Cys41 (3.6 Å). The distance between the Cys38 Sγ and the His40 Nδ1 is 3.9 Å, 0.3 Å longer than the equivalent distance found in reduced *Ec*DsbA (*6*). Electrostatic interaction between these two residues has been proposed as critical for stabilization of reduced DsbA. The corresponding histidine in oxidized *Vc*DsbA shows a different rotamer (Figure 2) and does not interact with the N-terminal catalytic cysteine. Interestingly, *Xf*DsbA Cys38 thiolate is further stabilized by a hydrogen bond with the side chain of Thr157 (3.1 Å distance). This residue, which precedes the highly conserved *cis*-Pro158 (Supporting Information Figure S1), is replaced by a structurally equivalent valine in *Ec*DsbA and *Vc*DsbA (Figure 2). A V*c*P motif is more conserved among the oxidases from Gram-negative bacteria, whereas the T*c*P motif is characteristic of isomerases like DsbC and DsbG. In the *Ec*DsbA structure the main chain of Val150 indirectly interacts with Cys30 Sγ through a water molecule, which has been proposed to be displaced by the substrate binding (*28*). Besides, *Xf*DsbA possesses two additional histidine residues in the vicinity of the CPHC motif; His43 is replaced by a glutamine in *Ec*DsbA and a threonine in *Vc*DsbA, whereas His100 is conserved in *Vc*DsbA but replaced by a glutamine residue in *Ec*DsbA (Figure 2).

Structural comparison of *Xf*DsbA and DsbL active sites shows that among the three DsbL distal lysines (Lys108, Lys177, Lys180) contributing to the net positive charge proposed to stabilize the Cys29thiolate in DsbL (*8*), only Lys177 has a corresponding positively charged residue in *Xf*DsbA (His171). On the other hand, the positive charges found at the active site neighborhood of DsbL are partially conserved in *Xf*DsbA. DsbL Lys34 is structurally equivalent to *Xf*DsbA His43, and DsbL His105 is conserved in *Xf*DsbA (His100). In contrast, *Xf*DsbA does not conserve a positively charged residue at the position of DsbL Lys61, which is structurally replaced by *Xf*DsbA Trp72. Additionally, the solvent-accessible DsbL Lys97 which was proposed by Grimshaw and colleagues to participate in the proton transfer to the C-terminal cysteine Cys32 (*8*) is replaced by His92 in *Xf*DsbA. Interestingly, the hydrogen bond network involving DsbL Lys97 and Cys32 is conserved in *Xf*DsbA through His92 and Cys41 (not shown).

Peptide Binding. During the last cycles of refinement, the Fourier difference maps clearly showed an elongated electron density at the surface of monomer C of *Xf*DsbA, close to the active site. The electron density was first interpreted as corresponding to a polyethylene glycol (PEG) molecule derived from the crystallization solution, but an ethylene glycol polymer did not fit well to the electron density after refinement. We thus considered the possibility that a molecule derived from the expression system had been copurified with *Xf*DsbA, and further analysis of the electron density maps indicated a polypeptide chain as the most probable choice. Besides the shape of the electron density, the interacting region corresponds to the DsbA hydrophobic groove which has been proposed to be involved in the substrate binding (*31*). In fact, an 8-mer peptide could be modeled with good refinement statistics (R_{free} dropped from 0.241 to 0.235 after refinement), and all residues fell in the allowed regions of the Ramachandran plot. Alanine side chains were placed at positions 1 to 5 and 8, whereas glycine residues were modeled at positions 6 and 7 (Figure 3). The modeled polypeptide is involved in hydrophobic contacts with *Xf*DsbA residues Cys38, His40, Phe68, Trp72, Leu150, Gly156, Asp172, and Phe173, besides interacting with the main chain of residues Val155 and Thr157 via hydrogen bonds. Interestingly, an extra density is observed at position 4 pointing to the Cys38 side chain, which may indicate a specific interaction. However, the quality of the electron density map does not allow defining the sequence of the polypeptide chain and thus analyzing specific interactions between the side chains (Figure 3). While attempting to solve the *Xf*DsbA structure, X-ray data from several crystals were collected, and in order to further investigate the presence of a ligand in the *Xf*DsbA active site, we afterward refined the structure against all of the available data sets. Electron density maps systematically revealed extra density close to the same region of the protein, which was more or less continuous depending on the data set. On the basis of the crystallographic data, we are not able to determine whether the additional density encountered is produced by a disordered peptide or a mixture of various peptides, but it appears that the average occupancy of the protein hydrophobic groove by a copurified peptide was dependent on the protein lot. Curiously, continuous density was only observed in the monomer C groove,

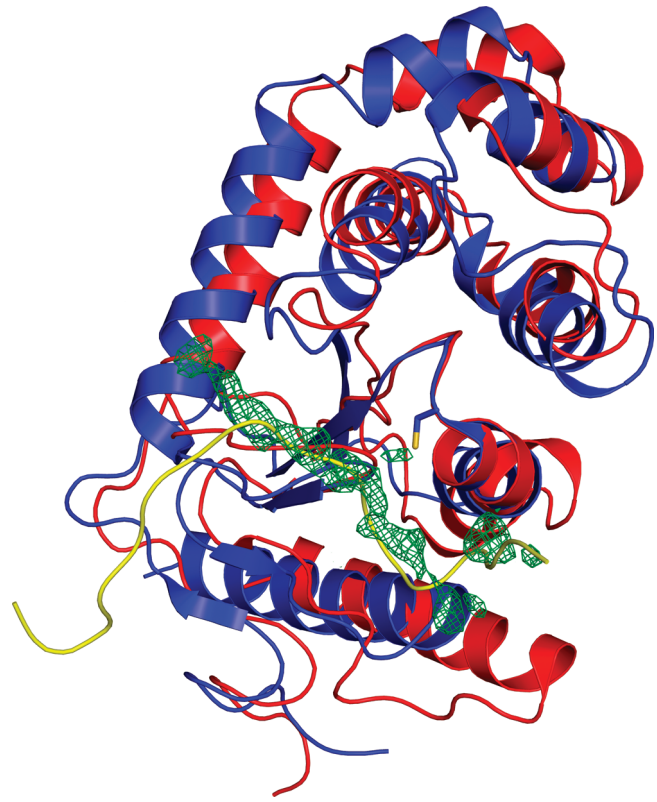

FIGURE 4: Superposition of the *Xf*DsbA structure and the complex *Ec*DsbA−DsbB. *Xf*DsbA and *Ec*DsbA are shown in blue and red, respectively, and the DsbB loop which interacts with *Ec*DsbA is represented in yellow. $F_o - F_c$ map contoured at 3σ (green) indicates the putative peptide binding site of *Xf*DsbA, which is in good agreement with the *Ec*DsbA−DsbB interaction region. Cys38 of *Xf*DsbA is indicated. *Ec*DsbA−DsbB atomic coordinates used in the superposition are available in the Protein Data Bank with the accession number 3E9J (*31*).

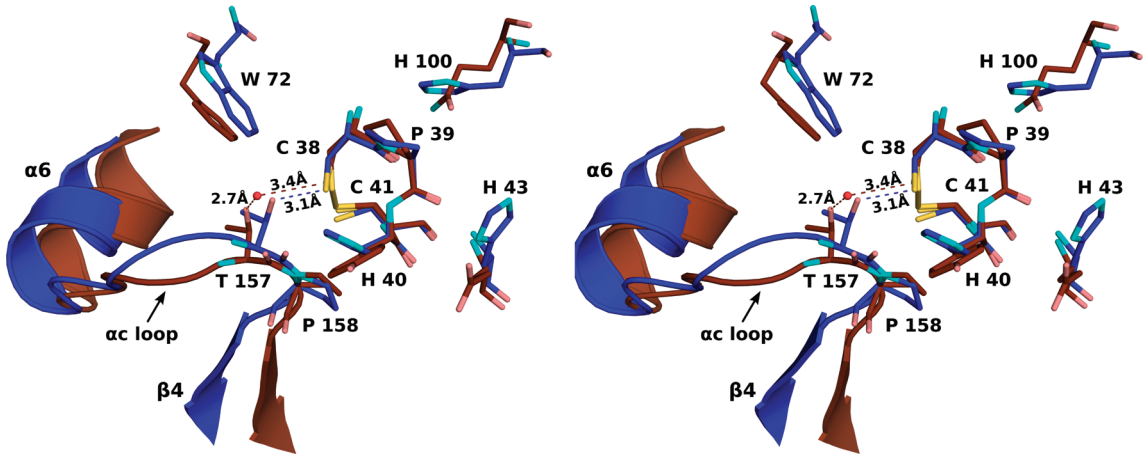

FIGURE 5: Stereoview of superposition of *Xf*DsbA (blue) and *Sa*DsbA (brown) active sites. The conformational change in the αc loop is shown, and the interaction distances involving the threonine residues of the T*c*P motif and the N-terminal catalytic cysteine are indicated. The water molecule that mediates this interaction in *Sa*DsbA is represented by a red sphere. Residues labels refer to *Xf*DsbA.

and we speculate that crystallization process may have selected and arranged the different molecules' population.

A strong extra density was also observed close to the Phe173 side chain (Figure 3). Attempts to fit a molecule derived from the crystal mother liquor or the cryoprotectant were unsuccessful, and we speculate that this density may also correspond to a small peptide fragment, probably a disordered extension of the refined 8-mer peptide. However, we were not able to find a model which unambiguously fitted the electron density map.

The crystal structures of the *E. coli* DsbA-DsbB$_{Cys130Ser}$ and DsbA-DsbB wild-type complexes were recently reported (*29, 30*). Interaction between the two proteins involves the second periplasmic loop of *Ec*DsbB (Pro100−Phe106), which is accommodated in the DsbA hydrophobic groove, below the catalytic Cys30. Cys104 from *Ec*DsbB forms a disulfide with *Ec*DsbA Cys30 during the DsbA−DsbB redox cycle. Additionally, structural studies on the *E. coli* DsbB protein by NMR revealed further details of DsbA−DsbB interaction (*32*). Besides the second periplasmic loop, DsbB residues 126−131 were identified as participating in the DsbA−DsbB complex formation through the interaction with the DsbA β3-α2 loop (*32*). Superposition of *Xf*DsbA structure and the complex *Ec*DsbA−DsbB (*30*) shows that the model of a polypeptide bound to the *Xf*DsbA monomer C is in good agreement with the conformation of the *Ec*DsbB loop which interacts with *Ec*DsbA (Figure 4). Notably, the tripeptide of *Ec*DsbA (Arg148-Gly149-Val150) which forms a short antiparallel β-sheet with *Ec*DsbB peptide Cys104−Phe106 (*29, 30*) has an equivalent in *Xf*DsbA, formed by residues Val155-Gly156-Thr157. *Xf*DsbA Val155 and Thr157 make hydrogen bonds with the main chain of the 8-mer peptide whereas the highly conserved Gly156 is involved in hydrophobic contacts with the ligand (Figure 3). In addition, the extra density observed close to the Phe173 side chain (mentioned above) also agrees with the DsbB loop conformation (Figure 4) and may indeed correspond to a disordered fragment of the polypeptide chain. Superposition of *Xf*DsbA structure with an *E. coli* DsbA−DsbB model which replaces the DsbB crystal structure with the NMR structure (*32*) shows that interaction between DsbB residues 126−131 and DsbA β3-α2 loop is also observed with *Xf*DsbA (not shown). Interestingly, the *Xf*DsbA β3-α2 loop comprises the residues

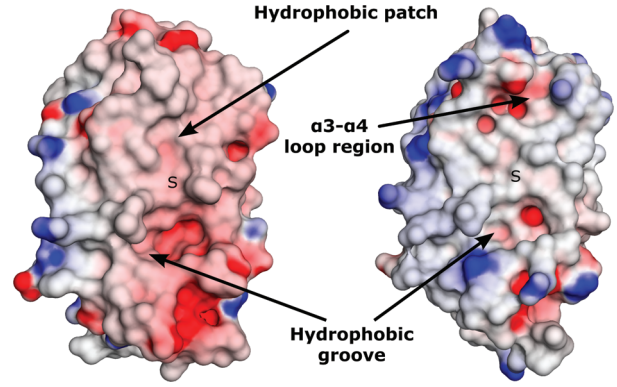

FIGURE 6: Electrostatic surfaces of *Xf*DsbA (left) and *Xf*DsbA2 (right) colored by charge from red (−17.5 kV) to blue (+17.5 kV). The position of the N-terminal catalytic cysteine is indicated by S. The hydrophobic patch observed in *Xf*DsbA and homologues from Gram-negative bacteria is not conserved in *Xf*DsbA2, mainly due to modifications at the α3-α4 loop region.

Phe68 and Trp72 which make hydrophobic interactions with the modeled 8-mer peptide (Figure 3).

Structural Comparison with DsbA from the Gram-Positive Bacterium S. aureus. Superposition of *Xf*DsbA and *Sa*DsbA structures results in an overall rms deviation of 3.1 Å for 154 Cα aligned. The main differences observed between *Sa*DsbA and *Ec*DsbA (*12*) are also verified in the comparison of *Sa*DsbA with *Xf*DsbA, notably, in the regions involved in the formation of the hydrophobic patch and groove present in Gram-negative homologues. Despite these differences, *Xf*DsbA shows an interesting similarity to its counterpart from Gram-positive *S. aureus*, not shared with the *E. coli* homologue. In both *Xf*DsbA and *Sa*DsbA a threonine residue replaces the valine in the conserved V*c*P motif. As mentioned before, *Xf*DsbA Thr157 forms a hydrogen bond with the N-terminal catalytic Cys38 whereas in *Sa*DsbA the interaction between the corresponding Thr153 and Cys26 is mediated by a water molecule (Figure 5). A conformational change at the αc loop that precedes the *cis*-Pro loop brings the *Xf*DsbA Thr157 closer to the active site cysteines in comparison with *Sa*DsbA structure (Figure 5). This region is directly involved in the substrate binding.

XfDsbA2, the Second Disulfide Oxidoreductase from X. fastidiosa. Analysis of the genome of *X. fastidiosa* (*10*) revealed the presence of two adjacent chromosomal genes

Table 2: Redox Potentials and DsbA/Glutathione Equilibrium Constants for *Xf*DsbA, *Xf*DsbA2, and the Respective Mutants *Xf*DsbAT157V and *Xf*DsbA2T203V at 30 °C[a]

		pH		
		6	7	8
K_{eq} (mM)	*Xf*DsbA	0.030 ± 0.008	0.014 ± 0.002	0.004 ± 0.001
	*Xf*DsbA2	0.035 ± 0.002	0.022 ± 0.003	0.008 ± 0.001
	*Xf*DsbAT157V		0.37 ± 0.04	
	*Xf*DsbA2T203V		0.48 ± 0.04	
E_0 (V)	*Xf*DsbA	−0.044 ± 0.003	−0.094 ± 0.002	−0.136 ± 0.008
	*Xf*DsbA2	−0.046 ± 0.001	−0.100 ± 0.002	−0.147 ± 0.001
	*Xf*DsbAT157V		−0.137 ± 0.001	
	*Xf*DsbA2T203V		−0.140 ± 0.001	
	GSSG/2GSH	−0.180	−0.240	−0.300

[a] The redox potential values of the glutathione redox couple used in the calculations are provided.

coding for two DsbA-like proteins. XF1436 (or *Xf*DsbA) belongs to the well-characterized DsbA family with the canonical motif CPHC, whereas the amino acid sequence of XF1437 shows a CPAC cluster at the active site. Although amino acid differences in the DsbA active site have already been observed (compiled in Quan et al. (*9*)), a similar case of two adjacent chromosomal *dsbA* genes had only been reported, to our knowledge, for the cold-adapted bacterium *Ph*TAC125 (*11*).

Both *X. fastidiosa* DsbA homologues possess the signal sequence, characteristic of secreted proteins. However, XF1437 (named *Xf*DsbA2) presents an extended N-terminal composed of 44 residues (see alignment in Supporting Information Figure S1), which does not show significant similarity to any other sequence when searched using the BLAST program (*33*). In addition, secondary structure prediction indicated that this N-terminal fragment is unfolded (data not shown).

Recombinant *Xf*DsbA2 was produced and purified. Characterization by circular dichroism (CD) showed minima in the CD spectra at 192, 209, and 222 nm, indicating a content of approximately 33% α-helix (Supporting Information Figure S3). Extensive attempts to crystallize *Xf*DsbA2 were unsuccessful, and in order to analyze its active site structure, a homology model was constructed. *Xf*DsbA2 model was built with the program MODELER (*25*) using the crystal structure of *Xf*DsbA as template. *Xf*DsbA and *Xf*DsbA2 sequences are 41% identical, and as expected, the overall structures are very similar, structural superposition resulting in rms deviation of 0.38 Å for 193 Cα aligned. A Ramachandran plot of *Xf*DsbA2 model is provided in Supporting Information Figure S4. The main difference in the global structure resides in the loop connecting helices α3 and α4. *Xf*DsbA2 has an insertion of two residues which results in a longer loop (Supporting Information Figure S5A). The active sites are also globally similar except for some residue substitutions. *Xf*DsbA2 Ala84 replaces the His40 of the *Xf*DsbA CPHC motif and *Xf*DsbA2 Gln87 substitutes *Xf*DsbA His43. Thr203 of *Xf*DsbA2 is in position to interact with the catalytic Cys82, similarly to Thr157 in *Xf*DsbA (Supporting Information Figure S5B). Interestingly, analysis of *Xf*DsbA and *Xf*DsbA2 electrostatic surfaces (Figure 6) shows that *Xf*DsbA2 lacks the well-characterized DsbA hydrophobic patch, which was shown to be involved in DsbA−DsbB interaction (*29, 30, 32*). The structural change observed in the loop linking helices α3 and α4 is mainly responsible for the difference between the molecular surfaces of *X. fastidiosa* DsbA homologues.

Redox Properties of XfDsbA and XfDsbA2. In order to verify if *Xf*DsbA2 is efficient as an oxidizing disulfide catalyst, the redox properties of *Xf*DsbA and *Xf*DsbA2 were studied by measuring the equilibrium constant of the DsbA/glutathione redox system (*4*). By plotting R against $[GSH]^2/[GSSG]$ (eq 1), the equilibrium constant K_{eq} is obtained after nonlinear regression (Supporting Information Figure S6). Equilibrium constants and redox potentials of *Xf*DsbA and *Xf*DsbA2 at 30 °C and pH 6.0, 7.0, and 8.0 are shown in Table 2. Surprisingly, the absence of the canonical CPHC motif in *Xf*DsbA2 does not appear to significantly affect its oxidizing power, since both enzymes have similar redox properties. Moreover, both *X. fastidiosa* enzymes were shown to be stronger oxidants than *Ec*DsbA, for which a redox potential of −0.120 V was measured at pH 7.0 (*5*). *Xf*DsbA redox potential (−0.094 V) is comparable to that of DsbL, recently characterized as the most oxidizing thioredoxin-like protein known (*8*).

Aiming at investigating the effect of the substitution of Thr157 and Thr203 residues on the oxidizing function of *Xf*DsbA and *Xf*DsbA2, respectively, we produced the mutants $Xf\text{DsbA}^{T157V}$ and $Xf\text{DsbA2}^{T203V}$ and determined their redox potentials (Table 2). Mutation of the threonine residues to a valine (residue present in the homologues *Ec*DsbA and *Vc*DsbA) caused a decrease in the redox potentials of *Xf*DsbA and *Xf*DsbA2 but did not abolish their oxidizing character. Comparison with the results obtained for *Ec*DsbA (*5*) shows that, in contrast to *X. fastidiosa* wild-type enzymes, *Xf*DsbA mutants are less oxidizing than their *E. coli* homologue.

DISCUSSION

The crystal structure of *X. fastidiosa* DsbA solved in this work, together with *Xf*DsbA2 homology model analysis and studies of redox activity of the wild-type enzymes and mutants, provides new information about the molecular basis for catalysis of thiol/disulfide exchange by DsbA family members. Modeling of a peptide bound to the active site of *Xf*DsbA monomer C allowed a detailed examination of DsbA residues putatively involved in substrate binding. Residues involved in the peptide binding come from both thioredoxin and helical DsbA domains. Extremities of the polypeptide are stabilized by hydrophobic contacts whereas the central tripeptide portion of the ligand closely interacts with *Xf*DsbA, via hydrogen bonds with the main chain of residues Val155 and Thr157 and hydrophobic contact with active site His40. These interactions may stabilize a favorable conformation for the intermolecular disulfide bond formation during the DsbA redox cycle.

Study of redox properties of *Xf*DsbA and *Xf*DsbA2 revealed that the substitution of the histidine residue of the CPHC motif did not significantly affect the oxidizing power of *Xf*DsbA2. In contrast, mutation of His32 in *Ec*DsbA led to a dramatic decrease of redox potential, making DsbA a less potent donor of disulfide bonds (*7*). This residue has been proposed to be essential for stabilization of the reduced form of DsbA, through electrostatic interaction with the N-terminal cysteine thiolate (*34*). Our observation that the introduction of mutations T157V and T203V in *Xf*DsbA and *Xf*DsbA2, respectively, decreased the oxidizing power of the enzymes indicates that, although not essential for the DsbA oxidative function, the threonine residue of the T*c*P motif may have a role in the stabilization of the Cys thiolate. The low pK_a of the N-terminal cysteine is also a determinant of the high oxidizing power of DsbA, and the residues which compose the active site environment are directly involved in maintaining this property (*7*). Besides the histidine from the CPHC motif, a glutamine residue has been proposed to influence the pK_a and the stability of the N-terminal cysteine thiolate (Gln97 in *Ec*DsbA) (*35, 36*). *Ec*DsbA Gln97, which belongs to the helical domain, is replaced by histidine in *Xf*DsbA (His100) and *Xf*DsbA2 (His144) (Figure 2 and Supporting Information Figure S4B). In *Xf*DsbA, His100 Nϵ2 is at 3.6 Å of the main chain oxygen of Cys38. Analysis of the sequences of DsbA family members shows that a histidine residue is more conserved at this position than a glutamine (Supporting Information Figure S1). The function of *Xf*DsbA2 as a potent oxidase indicates that the violation of the DsbA canonical motif CPHC may be compensated by residue substitutions within or at the vicinity of the active site. We propose that, in *X. fastidiosa* enzymes (*Xf*DsbA/*Xf*DsbA2), together with the Thr157/203 residues, His100/144 may contribute to the stabilization of Cys38/82 thiolate.

Similarly to *Xf*DsbA2, DsbA from Gram-positive *S. aureus* contains a substitution in the active site CPHC motif (the histidine residue is replaced by a tyrosine) but keeps the oxidizing function characteristic of the DsbA family. Moreover, *Sa*DsbA also presents a T*c*P motif, characteristic of isomerases, instead of the V*c*P motif more conserved in the oxidases family. In contrast to what we observed for the *X. fastidiosa* homologues, the introduction of mutation T153V in *Sa*DsbA did not significantly affect the redox potential of the enzyme, which could be explained by the weaker interaction observed between *Sa*DsbA Thr153 and the N-terminal catalytic cysteine if compared with *Xf*DsbA (Figure 5). Nevertheless, the T153V single substitution conferred to *Sa*DsbA partial ability to catalyze insulin reduction, a reaction also catalyzed by *Ec*DsbA (*12*), corroborating that the *cis*-Pro loop is involved in substrate binding. Despite the structural and functional differences between DsbA from Gram-positive *S. aureus* and its counterparts from Gram-negative bacteria (*12*), the presence of a T*c*P motif in DsbA proteins from both bacterial categories (for instance, *Sa*DsbA and *Xf*DsbA) appears to reveal a further link between enzymes from oxidase and isomerase families, more related with substrate binding than with specific enzymatic activity. In addition, analysis of *Xf*DsbA, *Ec*DsbA, *Vc*DsbA, and *Sa*DsbA structures shows that, despite the overall similarity, major differences reside in regions putatively involved in substrate interaction, suggesting that although keeping similar redox potentials, substrate specificity can significantly vary among DsbA family members even inside the same bacterial category.

Finally, the presence of two adjacent chromosomal genes coding for DsbA-like proteins is unusual for organisms, and to our knowledge, only one case had been reported (*11*). The cold-adapted bacterium *P. haloplanktis* (*Ph*TAC125) has two chromosomal *dsbA* genes organized in a functional operon, and similarly to what is observed in *X. fastidiosa*, *Ph*DsbA2 protein possesses a CPAC motif instead of the conserved CPHC (*11*). The redox properties of *Ph*DsbA2 remain to be determined, but comparison of amino acid sequences of *Xf*DsbA2 and *Ph*DsbA2 shows that the threonine residue proposed to contribute to stabilization of reduced *Xf*DsbA2 is not conserved in *Ph*DsbA2, which presents the more conserved valine residue in this position (Supporting Information Figure S1). The genome of *Xanthomonas axonopodis* (*37*), a plant pathogen from the same family of *X. fastidiosa*, also reveals two adjacent chromosomal genes encoding two oxidoreductases belonging to the DsbA family (codes XAC0722 and XAC0723). Curiously, in *X. axonopodis*, the protein which contains the canonical motif CPHC is encoded by the downstream ORF (XAC0723) in contrast to what is observed in *X. fastidiosa* and *Ph*TAC125. *Xf*DsbA and *Xf*DsbA2 share 59% and 67% identity with their counterparts from *X. axonopodis* (*Xa*DsbA and *Xa*DsbA2), and sequence analysis shows that the residues proposed to compensate for the absence of the active site histidine are conserved in *Xa*DsbA2 (Supporting Information Figure S1), suggesting that *Xa*DsbA2 may also have a role as disulfide catalyst. What is the specific function and mechanism of both proteins in the bacterial oxidative pathway is a question that remains to be answered, but the differences observed on the electrostatic surface of *Xf*DsbA and *Xf*DsbA2 could indicate that the two proteins have different substrate specificities. Analysis of the *X. fastidiosa* genome shows the presence of DsbB protein, which forms the redox pair with DsbA in the disulfide bond oxidative pathway, DsbC and DsbD proteins, which compose the thiol/disulfide isomerization pathway, and DsbE, which participates in the maturation process of *c*-type cytochromes (*1*). Nevertheless, *X. fastidiosa* lacks the genes encoding for DsbG, DsbL, and DsbI proteins. DsbL−DsbI is a newly identified redox pair participating in the oxidative pathway and has been proposed to have a limited set of specific substrates, including the arylsulfate sulfotransferase enzyme (*8*), which is also absent from *X. fastidiosa*. In contrast, DsbG participates in the DsbC/DsbG−DsbD isomerase pathway, and structural analysis suggested that DsbG may act later than its homologue DsbC in the protein folding process, catalyzing disulfide rearrangement in partially folded proteins (*38*). The lack of a DsbG protein in *X. fastidiosa* raises the question whether the thiol/disulfide isomerization pathway in *X. fastidiosa* relies only in DsbC−DsbD proteins. Heras and co-workers had proposed that the presence of the conserved threonine residue in the DsbC and DsbG *cis*-Pro loop might facilitate the isomerization activity, by increasing the resolution time of the mixed disulfide bond with the target protein and favoring formation of correct disulfide bonds (*38*). We are tempted to speculate about whether the T*c*P motif in *Xf*DsbA proteins also favors the catalysis of correct disulfide bonds, and the presence of two DsbA proteins in *X. fastidiosa* fills at some extent the lack of DsbG isomerase.

Very recently, structural and biochemical characterization of DsbA3 from *Neisseria meningitides* (*Nm*DsbA3) was reported (*39*). Interestingly, the conformation of the *Nm*DsbA3 active site CXXC motif, which is composed by a CVHC motif, is located in an extended loop preceding helix α1, in contrast to its counterparts from Gram-negative and Gram-positive bacteria where the CXXC motif forms the first turn of helix α1 (*39*). Results presented by Vivian and colleagues (*39*) are in accordance with the conclusions of our work in the sense that, except for the conformation of the active site CXXC motif, major differences in the *Nm*DsbA3 structure reside in the regions involved in the formation of the hydrophobic patch and groove. Moreover, similarly to *Sa*DsbA and *Xf*DsbA, *Nm*DsbA presents a threonine in the *cis*-Pro loop but keeps the oxidase activity (*39*).

Concluding, structural and functional studies on DsbA family members available so far indicate that structural variability of the regions putatively involved in substrate interaction, in particular the α2-β3, α3-α4, α6-β4 loops, and in the C-terminal α7, confers different substrate specificity among DsbA family members. Furthermore, sequence variability of the CXXC motif and residue substitutions at the active site neighborhood suggest that the redox potential of DsbA enzymes may rely on a more intricate interaction network, involving polar residues which do not interact directly with the side chain of the N-terminal catalytic cysteine.

ACKNOWLEDGMENT

We thank Celisa C. Tonoli and Zildene G. Correa for technical assistance, Amadeu H. Iglesias and Dr. Fábio Gozzo for assistance in the mass spectrometry analysis, and Dr. João Alexandre Barbosa for critical reading of the manuscript. We are grateful to Dr. Robert Sweet, Dr. Annie Heroux, and Dr. Desigan Kumaran for assistance in data collection at the NSLS.

SUPPORTING INFORMATION AVAILABLE

Figure S1, sequence alignment of DsbA family members; Figure S2, structural superposition of active site residues of *Xf*DsbA monomers; Figure S3, circular dichroism spectra of *Xf*DsbA and *Xf*DsbA2 proteins; Figure S4, Ramachandran plot of *Xf*DsbA2 model; Figure S5, superposition of the crystal structure of *Xf*DsbA and *Xf*DsbA2 homology model; Figure S6, redox equilibrium curves of wild-type *Xf*DsbA and *Xf*DsbA2 and mutants with glutathione; Figure S7, atomic coordinates of the *Xf*DsbA2 model. This material is available free of charge via the Internet at http://pubs.acs.org.

REFERENCES

1. Bader, M. W., and Bardwell, J. C. (2001) Catalysis of disulfide bond formation and isomerization in *Escherichia coli*. *Adv. Protein Chem. 59*, 283–301.
2. Bardwell, J. C. A., McGovern, K., and Beckwith, J. (1991) Identification of a protein required for disulfide bond formation *in vivo*. *Cell 67*, 6581–6589.
3. Martin, J. L., Bardwell, J. C., and Kuriyan, J. (1993) Crystal structure of the DsbA protein required for disulphide bond formation in vivo. *Nature 365*, 464–468.
4. Wunderlich, M., and Glockshuber, R. (1993) Redox properties of protein disulfide isomerase (DsbA) from *Escherichia coli*. *Protein Sci. 2*, 717–726.
5. Zapun, A., Bardwell, J. C. A., and Creighton, T. E. (1993) The reactive and destabilizing disulfide bond of DsbA, a protein required for protein disulfide bond formation in vivo. *Biochemistry 32*, 5083–5092.
6. Guddat, L. W., Bardwell, J. C. A., and Martin, J. L. (1998) Crystal structures of reduced and oxidized DsbA: investigation of domain motion and thiolate stability. *Structure 6*, 757–767.
7. Grauschopf, U., Winther, J. R., Korber, P., Zander, T., Dallinger, P., and Bardwell, J. C. A. (1995) Why is DsbA such an oxidizing disulfide catalyst? *Cell 83*, 947–955.
8. Grimshaw, J. P., Stirnimann, C. U., Brozzo, M. S., Malojcic, G., Grütter, M. G., Capitani, G., and Glockshuber, R. (2008) DsbL and DsbI form a specific dithiol oxidase system for periplasmic arylsulfate sulfotransferase in uropathogenic *Escherichia coli*. *J. Mol. Biol. 380*, 667–80.
9. Quan, S., Schneider, I., Pan, J., Hacht, A. V., and Bardwell, J. C. A. (2007) The CXXC motif is more than a redox rheostat. *J. Biol. Chem. 282*, 28823–28833.
10. Simpson, A. J. G., Reinach, F. C., Arruda, P., Abreu, F. A., Acencio, M., Alvarenga, R., Alves, L. M., Araya, J. E., Baia, G. S., Baptista, C. S., Barros, M. H., Bonaccorsi, E. D., Bordin, S., Bove, J. M., Briones, M. R., Bueno, M. R., Camargo, A. A., Camargo, L. E., Carraro, D. M., Carrer, H., Colauto, N. B., Colombo, C., Costa, F. F., Costa, M. C., Costa-Neto, C. M., Coutinho, L. L., Cristofani, M., Dias-Neto, E., Docena, C., El-Dorry, H., Facincani, A. P., Ferreira, A. J., Ferreira, V. C., Ferro, J. A., Fraga, J. S., Franca, S. C., Franco, M. C., Frohme, M., Furlan, L. R., Garnier, M, Goldman, G. H., Goldman, M. H., Gomes, S. L., Gruber, A., Ho, P. L., Hoheisel, J. D., Junqueira, M. L., Kemper, E. L., Kitajima, J. P., Krieger, J. E., Kuramae, E. E., Laigret, F., Lambais, M. R., Leite, L. C. C., Lemos, E. G., Lemos, M. V., Lopes, S. A., Lopes, C. R., Machado, J. A., Machado, M. A., Madeira, A. M., Madeira, H. M., Marino, C. L., Marques, M. V., Martins, E. A., Martins, E. M., Matsukuma, A. Y., Menck, C. F., Miracca, E. C., Miyaki, C. Y., Monteiro-Vitorello, C. B., Moon, D. H., Nagai, M. A., Nascimento, A. L., Netto, L. E. S., Nhani, A., Jr., Nobrega, F. G., Nunes, L. R., Oliveira, M. A., de Oliveira, M. C., de Oliveira, R. C., Palmieri, D. A., Paris, A., Peixoto, B. R., Pereira, G. A. G., Pereira, H. A., Jr., Pesquero, J. B., Quaggio, R. B., Roberto, P. G., Rodrigues, V., de M. Rosa, A. J., de Rosa, V. E. Jr., de Sa, R. G., Santelli, R. V., Sawasaki, H. E., da Silva, A. C., da Silva, A. M., da Silva, F. R., da Silva, W. A., Jr., da Silveira, J. F., Silvestri, M. L., Siqueira, W. J., de Souza, A. A., de Souza, A. P., Terenzi, M. F., Truffi, D., Tsai, S. M., Tsuhako, M. H., Vallada, H., Van Sluys, M. A., Verjovski-Almeida, S., Vettore, A. L., Zago, M. A., Zatz, M., Meidanis, J., and Setubal, J. C. (2000) The genome sequence of the plant pathogen *Xylella fastidiosa*. *Nature 406*, 151–157.
11. Madonna, S., Papa, R., Birolo, L., Autore, F., Doti, N., Marino, G., Quemeneur, E., Sannia, G., Tutino, M. L., and Duilio, A. (2006) The thiol-disulfide oxidoreductase system in the cold-adapted bacterium *Pseudoalteromonas haloplanktis* TAC 125: discovery of a novel disulfide oxidoreductase enzyme. *Extremophiles 10*, 41–51.
12. Heras, B., Kurz, M., Jarrott, R., Shouldice, S. R., Frei, P., Robin, G., Cemazar, M., Thöny-Meyer, L., Glockshuber, R., and Martin, J. L. (2008) *Staphylococcus aureus* DsbA does not have a destabilizing disulfide. A new paradigm for bacterial oxidative folding. *J. Biol. Chem. 283*, 4261–4271.
13. Otwinowski, Z., and Minor, W. (1997) Processing of x-ray diffraction data collected in oscillation mode. *Methods Enzymol. 276*, 307–326.
14. Matthews, B. W. (1968) The solvent content of protein crystals. *J. Mol. Biol. 33*, 491–497.
15. Sheldrick, G., and Schneider, T. (1997) SHELXL: high-resolution refinement. *Methods Enzymol. 277*, 319–343.
16. de la Fortelle, E., and Bricogne, G. (1997) Maximum-likelihood heavy-atom parameter refinement for multiple isomorphous replacement and multiwavelength anomalous diffraction methods. *Methods Enzymol. 276*, 472–494.
17. Abrahams, J. P., and Leslie, A. G. W. (1996) Methods used in the structure determination of bovine mitochondrial F1 ATPase. *Acta Crystallogr., Sect. D: Biol. Crystallogr. 52*, 30–42.
18. Perrakis, A., Morris, R. J., and Lamzin, V. S. (1999) Automated protein model building combined with iterative structure refinement. *Nat. Struct. Biol. 6*, 458–463.
19. Murshudov, G. N., Vagin, A. A., and Dodson, E. J. (1997) Refinement of macromolecular structures by the maximum-

likelihood method. *Acta Crystallogr., Sect. D: Biol. Crystallogr. 53*, 240–255.
20. Emsley, P., and Cowtan, K. (2004) Coot: model-building tools for molecular graphics. *Acta Crystallogr., Sect. D: Biol. Crystallogr. 60*, 2126–2132.
21. Painter, J., and Merritt, E. A. (2006) Optimal description of a protein structure in terms of multiple groups undergoing TLS motion. *Acta Crystallogr., Sect. D: Biol. Crystallogr. 62*, 439–450.
22. Laskowski, R. A., MacArthur, M. W., Moss, D. S., and Thornton, J. M. (1993) PROCHECK: a program to check the stereochemical quality of protein structures. *J. Appl. Crystallogr. 26*, 283–291.
23. DeLano, W. L. (2002) The PyMOL Molecular Graphics System, DeLano Scientific, San Carlos, CA.
24. Rost, J., and Rapoport, S. (1964) Reduction-potential of glutathione. *Nature 201*, 185–185.
25. Šali, A., and Blundell, T. L. (1993) Comparative protein modeling by satisfaction of spatial restraints. *J. Mol. Biol. 234*, 779–815.
26. Luthy, R., Bowie, J. U., and Eisenberg, D. (1992) Assessment of protein models with three-dimensional profiles. *Nature 356*, 83–85.
27. Pontius, J., Richelle, J., and Wodak, S. J. (1996) Deviations from standard atomic volumes as a quality measure for protein crystal structures. *J. Mol. Biol. 264*, 121–136.
28. Hu, S. H., Peek, J. A., Rattigan, E., Taylor, R. K., and Martin, J. L. (1997) Structure of TcpG, the DsbA protein folding catalyst from *Vibrio cholera*. *J. Mol. Biol. 268*, 137–146.
29. Inaba, K., Murakami, S., Suzuki, M., Nakagawa, A., Yamashita, E., Okada, K., and Ito, K. (2006) Crystal structure of the DsbB-DsbA complex reveals a mechanism of disulfide bond generation. *Cell 127*, 789–801.
30. Malojcí, G., Owen, R. L., Grimshaw, J. P., and Glockshuber, R. (2008) Preparation and structure of the charge-transfer intermediate of the transmembrane redox catalyst DsbB. *FEBS Lett. 582*, 3301–3307.
31. Guddat, L. W., Bardwell, J. C. A., Zander, T., and Martin, J. L. (1997) The uncharged surface features surrounding the active-site of *Escherichia coli* DsbA are conserved and are implicated in peptide binding. *Protein Sci. 6*, 1148–1156.
32. Zhou, Y., Cierpicki, T., Jimenez, R. H., Lukasik, S. M., Ellena, J. F., Cafiso, D. S., Kadokura, H., Beckwith, J., and Bushweller, J. H. (2008) NMR solution structure of the integral membrane enzyme DsbB: functional insights into DsbB-catalyzed disulfide bond formation. *Mol. Cell 31*, 896–908.
33. Altschul, S. F., Gish, W., Miller, W., Myers, E. W., and Lipman, D. J. (1990) Basic local alignment search tool. *J. Mol. Biol. 215*, 403–410.
34. Guddat, L. W., Bardwell, J. C. A., Glockshuber, R., Wunderlich, M., Zander, T., and Martin, J. L. (1997) Structural analysis of three His32 mutants of DsbA: support for an electrostatic role of His32 in DsbA stability. *Protein Sci. 6*, 1893–1900.
35. Hawkins, H. C., de Nardi, M., and Freedman, R. B. (1991) Redox properties and cross-linking of the dithiol/disulphide active sites of mammalian protein disulphide-isomerase. *Biochem. J. 275*, 341–348.
36. Gane, P. J., Freedman, R. B., and Warwicker, J. (1995) A molecular model for the redox potential difference between thioredoxin and DsbA, based on electrostatics calculations. *J. Mol. Biol. 249*, 376–387.
37. da Silva, A. C. R., Ferro, J. A., Reinach, F. C., Farah, C. S., Furlan, L. R., Quaggio, R. B., Monteiro-Vitorello, C. B., Sluys, M. A. Van, Almeida, N. F., Alves, L. M. C., do Amaral, A. M., Bertolini, M. C., Camargo, L. E. A, Camarotte, G., Cannavan, F., Cardozo, J., Chambergo, F., Ciapina, L. P., Cicarelli, R. M. B., Coutinho, L. L., Cursino-Santos, J. R., El-Dorry, H., Faria, J. B., Ferreira, A. J. S., Ferreira, R. C. C., Ferro, M. I. T., Formighieri, E. F., Franco, M. C., Greggio, C. C., Gruber, A., Katsuyama, A. M., Kishi, L. T., Leite, R. P., Lemos, E. G. M., Lemos, M. V. F., Locali, E. C., Machado, M. A., Madeira, A. M. B. N., Martinez-Rossi, N. M., Martins, E. C., Meidanis, J., Menck, C. F. M., Miyaki, C. Y., Moon, D. H., Moreira, L. M., Novo, M. T. M., Okura, V. K., Oliveira, M. C., Oliveira, V. R., Pereira, H. A., Rossi, A., Sena, J. A. D., Silva, C., de Souza, R. F., Spinola, L. A. F., Takita, M. A., Tamura, R. E., Teixeira, E. C., Tezza, R. I. D., Trindade dos Santos, M., Truffi, D., Tsai, S. M., White, F. F., Setubal, J. C., and Kitajima, J. P. (2002) Comparison of the genomes of two *Xanthomonas* pathogens with differing host specificities. *Nature 417*, 459–463.
38. Heras, B., Edeling, M. A., Schirra, H. J., Raina, S., and Martin, J. L. (2004) Crystal structures of the DsbG disulfide isomerase reveal an unstable disulfide. *Proc. Natl. Acad. Sci. U.S.A. 24*, 8876–8881.
39. Vivian, J. P., Scoullar, J., Robertson, A. L., Bottomley, S. P., Horne, J., Chin, Y., Wielens, J., Thompson, P. E., Velkov, T., Piek, S., Byres, E., Beddoe, T., Wilce, M. C., Kahler, C., Rossjohn, J., and Scanlon, M. J. (2008) Structural and biochemical characterization of the oxidoreductase NmDsbA3 from *Neisseria meningitidis*. *J. Biol. Chem. 283*, 32452–32461.

BI801899X